long wavelength (a 0.5-eV electron has a wavelength of about 2 nm) and may therefore interact coherently with a large area of the monolayer (*21*), hence, many chiral centers. This last effect is evident in the rapid loss of asymmetry when the monolayer film has a 1% dopant of its enantiomer. The results in Fig. 2B suggest that the latter effect is dominant for this system.

Two important implications of our results are sketched here. A solid substrate coated with a thin layer of chiral molecules could be used to generate highly polarized electron beams. For example, after an unpolarized beam of electrons transverses five layers of L-stearoyl lysine, it will contain twice as many "spin up" electrons as "spin down" ones. The second implication relates to the origin of chirality in nature. Early studies of the asymmetry in electron scattering from chiral molecules was motivated by the suggestion (*23*) that chiral asymmetry may arise through the preferential destruction of one enantiomer in a racemic mixture by spin-polarized electrons produced in β decay (*24*). Our results suggest that the electron mechanism for generating chiral asymmetry in nature may be viable if the molecules are oriented by adsorption or other means at an interface. In such structures, the enhanced asymmetry in the electron molecule scattering cross sections (compared with the gas phase) arises from cooperative phenomena related to the structure of monolayer films. It remains to be seen, however, if these asymmetric interactions can give rise to asymmetric chemical transformations.

References and Notes

1. L. Pasteur, *Ann. Chim. Phys*. **24**, 442 (1848).
2. C. Nolting, S. Mayer, J. Kessler, *J. Phys. B* **30**, 5491 (1997).
3. S. Mayer and J. Kessler, *Phys. Rev. Lett.* **74**, 4803 (1995).
4. A. Rich, J. Van House, R. A. Hegstrom, *ibid.* **48**, 1341 (1982).
5. M. J. M. Beerlage, P. S. Farago, M. J. Vanderwiel, *J. Phys. B* **14**, 3245 (1981).
6. R. A. Hegstrom, D. W. Rein, P. G. H. Sandars, *J. Chem. Phys.* **73**, 2329 (1980).
7. T. L. V. Ulbricht and F. Vester, *Tetrahedron* **18**, 629 (1962).
8. W. A. Bonner, M. A. Van Dort, M. R. Yearian, *Nature* **258**, 419 (1975).
9. K. Blum and D. G. Thompson, *Adv. At. Mol. Opt. Phys.* **38**, 39 (1997).
10. C. Johnston, K. Blum, D. Thompson, *J. Phys. B* **26**, 965 (1993).
11. D. G. Thompson and M. Kinnin, *ibid.* **28**, 2473 (1995).
12. I. M. Smith, D. G. Thompson, K. Blum, *ibid.* **31**, 4029 (1998).
13. S. Mayer, C. Nolting, J. Kessler, *ibid.* **29**, 3497 (1996).
14. A. Kadyshevitch and R. Naaman, *Phys. Rev. Lett.* **74**, 3443 (1995).
15. R. Popovitz-Biro *et al.*, *J. Am. Chem. Soc.* **112**, 2498 (1990).
16. Y. Paz, S. Trakhtenberg, R. Naaman, *J. Phys. Chem.* **96**, 10964 (1992).
17. J. Kirschner, *Polarized Electrons at Surfaces*, (Springer-Verlag, Berlin, Germany, 1985).
18. F. Meier and D. Pescia, *Phys. Rev. Lett.* **47**, 374 (1981).
19. F. Meier, G. L. Bona, S. Hufner, *ibid.* **52**, 1152 (1984); G. Borstel and M. Wohlecke, *Phys. Rev. B* **26**, 1148 (1982).
20. Although close to the error in the quantum yield measurement (~5% for comparisons between samples), the transmission for the 1L2D2L structure may be higher than that of the 3L2D structure. This behavior can result from consideration of the phase terms in describing the electron transmission through the film. See (*9*–*11*).
21. A. Kadyshevitch, S. P. Ananthavel, R. Naaman, *J. Chem. Phys.* **107**, 1288 (1997).
22. R. Naaman, A. Haran, A. Nitzan, D. Evans, M. Galperin, *J. Phys. Chem. B* **102**, 3658 (1998).
23. F. Vester, T. L. V. Ulbricht, H. Krauch, *Naturwissenschaften* **46**, 68 (1959); T. L. V. Ulbricht, *Q. Rev.* **13**, 48 (1959).
24. W. A. Bonner, *Origins Life Evol. Biosphere* **21**, 59 (1991).

25. We thank J. Frey and M. Lahav for providing the L/D-stearoyl lysine. D.H.W. is the Belkin Visiting Professor at the Weizmann Institute. This work was partially supported by the Israel Science Foundation and by the MINERVA Foundation, Munich, Germany.

21 August 1998; accepted 23 December 1998

Self-Assembly of Flat Nanodiscs in Salt-Free Catanionic Surfactant Solutions

Th. Zemb,[1]* M. Dubois,[1] B. Demé,[2] Th. Gulik-Krzywicki[3]

Discs of finite size are a very rare form of stable surfactant self-assembly. It is shown that mixing of two oppositely charged single-chain surfactants can produce rigid nanodiscs as well as swollen lamellar liquid crystals with frozen bilayers. The crucial requirement for obtaining nanodisc self-assembly is the use of H^+ and OH^- as counterions. These counterions then form water and lower the conductivity to 10 microsiemens per centimeter. In the case of cationic component excess, a dilute solution of nanodiscs is in thermodynamic equilibrium with a lamellar phase. The diameter of the cationic nanodiscs is continuously adjustable from a few micrometers to 30 nanometers, with the positive charge located mainly around the edges.

Above the chain melting temperature, solutions of single-chain ionic surfactants self-assemble into micelles in water. A large number of stable shapes such as spheres, cylinders, and folded bilayers, but not flat finite discs, have been reported. If anionic and cationic surfactants are mixed (catanionic), the strong reduction in area per head group resulting from ion pairing induces formation of molecular bilayers at low concentrations. Thus, vesicles may form spontaneously. These vesicles are a thermodynamically stable state (*1*). The two counterions of the anionic and cationic surfactant form a dissociated salt. For a catanionic weight concentration of 5%, the resulting ionic strength exceeds 0.1 M. Vesicles as well as flexible cylinders have been identified and described in catanionic surfactant systems (*2, 3*). Because of the high ionic strength between aggregates, electrostatic repulsions are screened. The osmotic pressure of these aggregates is <100 Pa. In the absence of electrostatic repulsion stabilizing the system, the catanionic bilayers spontaneously form closed vesicles (*4*). Hoffmann *et al.* (*5*) have published a pioneering study of catanionic systems without excess salt; they have observed strongly repulsive charged cylinders of limited length.

Catanionic solutions described in the literature usually consist of five components, including the two counterions, with overall electroneutrality. The equilibrium-phase diagram at fixed temperature can then be represented in space in a tetrahedron containing the single-phase and multiple-phase regions (*6*). A highly stable colloidal solution requires a high osmotic pressure induced by unscreened electrostatic repulsions. This condition is met in pure catanionic surfactant solutions that contain only recombining H^+ and OH^- counterions plus counterions of the component in excess. In this case, the phase diagram can be approximated as a triangle, with only two degrees of freedom.

In this study, we obtained catanionic solutions by mixing myristic acid ($C_{13}H_{27}COO^-H^+$) and the hydroxide-exchanged form of cetyltrimethylammonium chloride [$C_{16}H_{33}N(CH_3)_3^+OH^-$] (*7*). Obtaining a pure carbonate-free surfactant solution requires the use of a glove box under nitrogen to avoid contact with atmospheric CO_2 (*7*). Near equimolarity, at a total surfactant content of 20 g/liter, the conductivity was on the order of 10 μS/cm, which corresponds to an ionic concentration on the order of 10 μM. The Debye screening length associated with this conductivity is about 100 nm, compared with 5 to 15 nm obtained with other counterions (*8*). The pH varied from 7

[1]Service de Chimie Moléculaire (Commissariat à l'Energie Atomique/Saclay), F-91191 Gif-sur-Yvette Cedex, France. [2]Institut Laue-Langevin, F-38042 Grenoble Cedex 9, France. [3]Centre de Génétique Moléculaire, Centre National de la Recherche Scientifique, F-91190 Gif-sur-Yvette, France.

*To whom correspondence should be addressed. E-mail: zemb@nanga.saclay.cea.fr

near equimolarity to 12 to 13 at large cationic surfactant excess. As counterions, the OH^- ions do not influence screening length.

In the absence of excess counterions, two quantities control the composition of the quasi-ternary system. The location of a sample in the ternary-phase triangle will be represented by using the total amount of dry surfactant c (in weight %) and the molar fraction of anionic surfactant r given by

$$r = [C_{13}COO^-H^+]/\{[C_{16}N(CH_3)_3{}^+OH^-] + [C_{13}COO^-H^+]\} \quad (1)$$

Myristic acid is insoluble in water; therefore we have focused our attention on compositions where cationic surfactant is in excess ($r < 0.5$; pH > 7). The conductivity is dominated by the excess hydroxide counterions and the monomeric cationic surfactant. When $r \rightarrow 0.5$, the surface charge density decreases. If we assume ideal mixing, the structural charge of the bilayer formed is given in charge per square nanometer by

$$Z = rA \text{ (cationic, solid)} + rA \text{ (anionic, solid)} + (1 - 2r)A \text{ (cationic, liquid)} \quad (2)$$

where the area per molecule A is close to 0.25 nm^2 when chains are solid and 0.6 nm^2 when chains are liquid (*6*). Cryofracture experiments were performed by the same procedure as in the swollen lamellar or vesicle phases of other cationic double-chain surfactant solutions (*8*), adding 30% glycerol (*9*)

First, we consider the case of a transparent nonbirefringent dilute sample ($c = 0.1\%$). Its appearance is quite different from other catanionic solutions, which have a bluish appearance when vesicles are formed. An exceptionally intense small-angle neutron scattering (SANS) signal decreasing as the second power of the scattering vector is produced (Fig. 1A, III). The power law behavior observed at the surfactant volume fraction in water (f) close to zero is q^{-2}, where $q = 4\pi/\lambda \sin(\theta)$, λ is the incident radiation wavelength, and θ is half the scattering angle. This indicates the existence of flat objects, at least in the micrometer range, because q^{-2} decay extends to $q < 8 \times 10^{-4}$ Å^{-1}. The local minimum at high q ($q = 0.15$ Å^{-1}) gives the bilayer thickness $2t = 4.2$ nm.

In the very low q range, static light-scattering measurements (Rayleigh ratio) also show q^{-2} behavior over the whole accessible angular range (Fig. 1B). Heating the sample to 50°C reduces the scattering by more than one order of magnitude. The strong initial light-scattering signal is completely restored after cooling back to room temperature. This reversibility demonstrates that the discs are dispersed at thermodynamic equilibrium. The in-plane coherence length is in the micrometer range (q^{-2} extends to $q < 8 \times 10^{-4}$ Å^{-1} with both light and neutron scattering). Increasing the concentration of the catanionic solution produces a clear birefringent gel. The observed interlamellar spacings of several hundred angstroms are unusual for frozen chains and are produced by lateral coalescence of discs. Five sharp Bragg reflections can be observed in Fig. 1A, II. Thus, bilayers are extremely stiff; no spacing out-of-plane fluctuations are detectable.

When the molar ratio is decreased to $r < 0.10$, an isotropic micellar phase of giant worm-like flexible micelles (L_1) forms, producing only a broad interaction peak at $q \approx 0.05$ Å^{-1} as indicated in Fig. 1A, I. The strong-intensity light scattering observed in this L_1 region indicates that micelles are giant flexible, and not small globular, objects, as expected from curvature theory, close to a lamellar phase region (*10*).

From the shape and position of the wide-angle x-ray scattering peak (Fig. 2) produced by the birefringent lamellar sample (Fig. 2) corresponding to the lateral interchain dis-

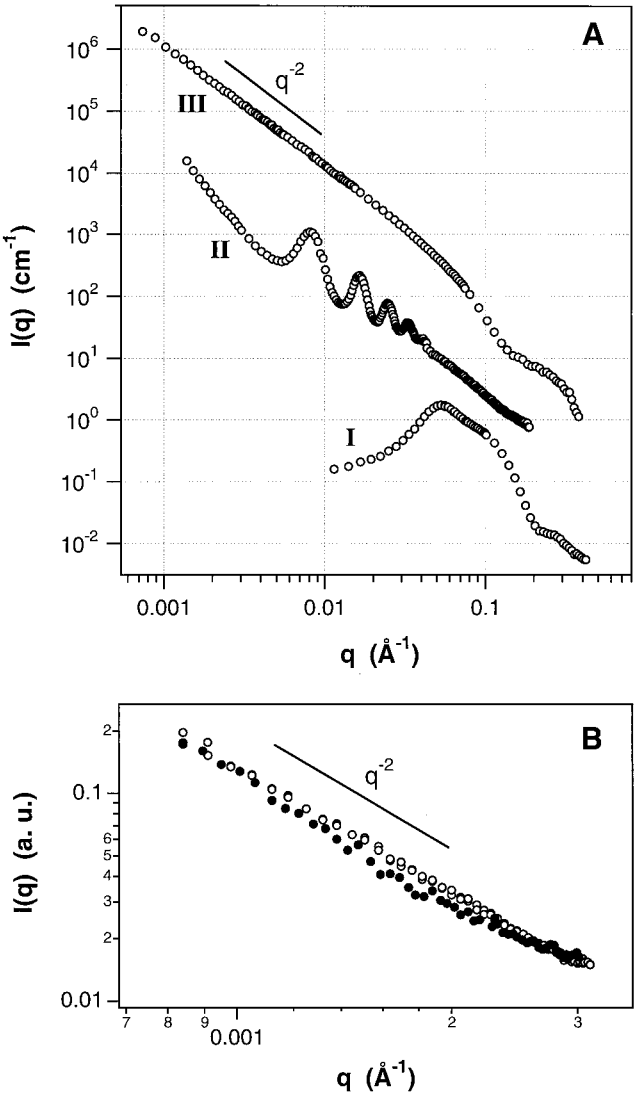

Fig. 1. (**A**) SANS (in absolute units, cm^{-1}) obtained with increasing surface charge. For decreasing surface charge (I to III), different microstructures are encountered: I, $r = 0.11$ and $c = 1.92\%$, strongly repulsive worm-like giant micelles form (L_1). II, $r = 0.305$ and $c = 0.76\%$, a swollen lamellar phase (L_β^+) of periodicity 78 nm is evidenced by five Bragg reflections (intensity scale × 10 for clarity). III, for $r \approx 0.5$ and $c = 3\%$, a dilute unbound dispersion of discs (U^+) is seen (intensity scale × 1000). (**B**) Reversibility of static light-scattering intensity versus scattering vector [log scale arbitrary units (a.u.)] equilibrated at room temperature ($r = 0.45$ and $c = 0.01\%$) before and after heating the sample to 60°C. The strong initial signal (decay as q^{-2}) is restored when large discs grow again during cooling.

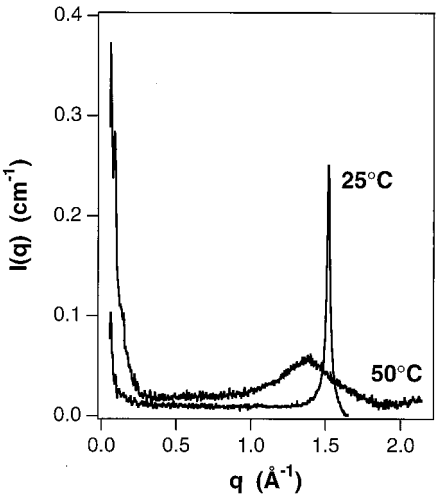

Fig. 2. Wide-angle x-ray scattering obtained on a Guinier-Mering camera with image plates. Sample composition: $r = 0.45$ and $c = 4\%$. Scattering curves at 25°C (sharp peak) and 50°C (broad peak) show the transition from frozen chains (L_β^+) to liquid chains (L_α^+).

tance of 4.2 Å in the bilayer, we conclude that the hydrocarbon chains are frozen (*11*). The peak at 1.5 $Å^{-1}$ corresponds to the lateral interchain distance of 4.2 Å in the bilayer. The swollen gel made of positively charged membranes is therefore labeled L_β^+. A two-dimensional array of alternating charges stabilizes the bilayer in a sandwich-like structure. The stiffness of the unbound discs produced in phase U^+ (unbound) by diluting the lamellar phase is deduced from the large q range where the q^{-2} behavior is observed. This power law extends to <0.001 $Å^{-1}$: the unbound nanodiscs appear flat on more than 1 μm in real space (Fig. 1A, III) and therefore have the same rigidity as catanionic bilayers.

We obtained freeze-fracture electron micrographs for rigid nanodiscs with increasing surface charge (Fig. 3). The electron micrographs focus on the coexistence between the swollen (L_β^+) phase and isolated discs. The size of the dispersed discs decreases when surface charge increases. Nanodiscs dispersed in a lamellar matrix at maximum swelling decrease from 3 mm to 30 nm when the molar ratio is decreased from 0.45 to 0.39 (Fig. 3, A to D). The lamellar phase in equilibrium with micelles is shown in Fig. 3E. A dispersion containing only micelles cannot be resolved by freeze-fracture electron microscopy (Fig. 3F).

The osmotic pressure of a catanionic sample for $c = 0.04\%$ and $r = 0.45$ was 500 ± 100 Pa (*12*). If this dispersion of nanodiscs were in a metastable state, the expected thermodynamic equilibrium phase at finite dilution would be a smectic phase in equilibrium with excess water. Thus, the total osmotic pressure would be close to zero (*13*). Samples showed no sign of sedimentation or phase separation after weeks of storage at room temperature in a sealed container. Under the same conditions, other catanionic systems in the presence of excess salt show closed vesicles as the equilibrium structures at high ionic strength (*1*). We can rationalize the high osmotic pressure in our samples as follows: the background electrolyte is the critical micellar concentration of the mixed surfactant, which is on the order of 30 μM. The surface potential, deduced from the Grahame equation (*10*), is on the order of 300 mV, and the measured osmotic pressure of the lamellar phase at maximum swelling (80 nm) is 500 Pa when it coexists with discs.

According to the thermodynamics of surfactant self-assembly, the stability of discs is very improbable because flat parts and highly curved edges must coexist in a single microstructure (*14*). How can catanionic nanodiscs be the most stable shape in the case described here? If the edges of the nanodiscs were not covered by surfactant, rigid nanodiscs of bilayers could form only at a high energetic cost, on the order of $\gamma(2\pi Dt)$, where γ is the oil-water surface tension, $2t$ is the disc thickness, and D is the disc diameter (*15*). The formation of nanodiscs described here requires ion pairing on faces coexisting with highly curved interfaces forming the edges. Adding excess cationic surfactant reduces the equilibrium size of the nanodiscs. Therefore, part of the excess cationic surfactant forms the edges of the discs. The final size is a balance between the entropy of mixing and electrostatic coupling between discs; increasing the excess charge favors small discs until the phase transition toward worm-like micelles (*16*). One of the consequences of this partial charge separation in the disc is that catanionic nanodiscs bear high-charge density at the strongly curved edges, in contrast to clay particles where edges are hydrophobic (*17*). The molar ratio of the two components gives us a direct way to control the diameter of the nanodisc.

On the basis of results obtained on more than 100 samples of different compositions ($0.1\% < c < 20\%$; $0.5 < r < 0$), prepared in the presence of atmospheric CO_2, we located the single-phase regions in the water-rich corner of the phase diagram (Fig. 4). However, in the absence of atmospheric CO_2, which decreases the conductivity of the sample to <10 μS/cm, a dilute isotropic solution (U^+) to nematic and then to smectic (L_β^+) phase sequence is observed with increasing concentration.

In the presence of CO_2, the maximum concentration where unbound freely rotating discs (U^+) are observed is $c = 0.1\%$. At $r \approx 0.5$, the lamellar phase in equilibrium with

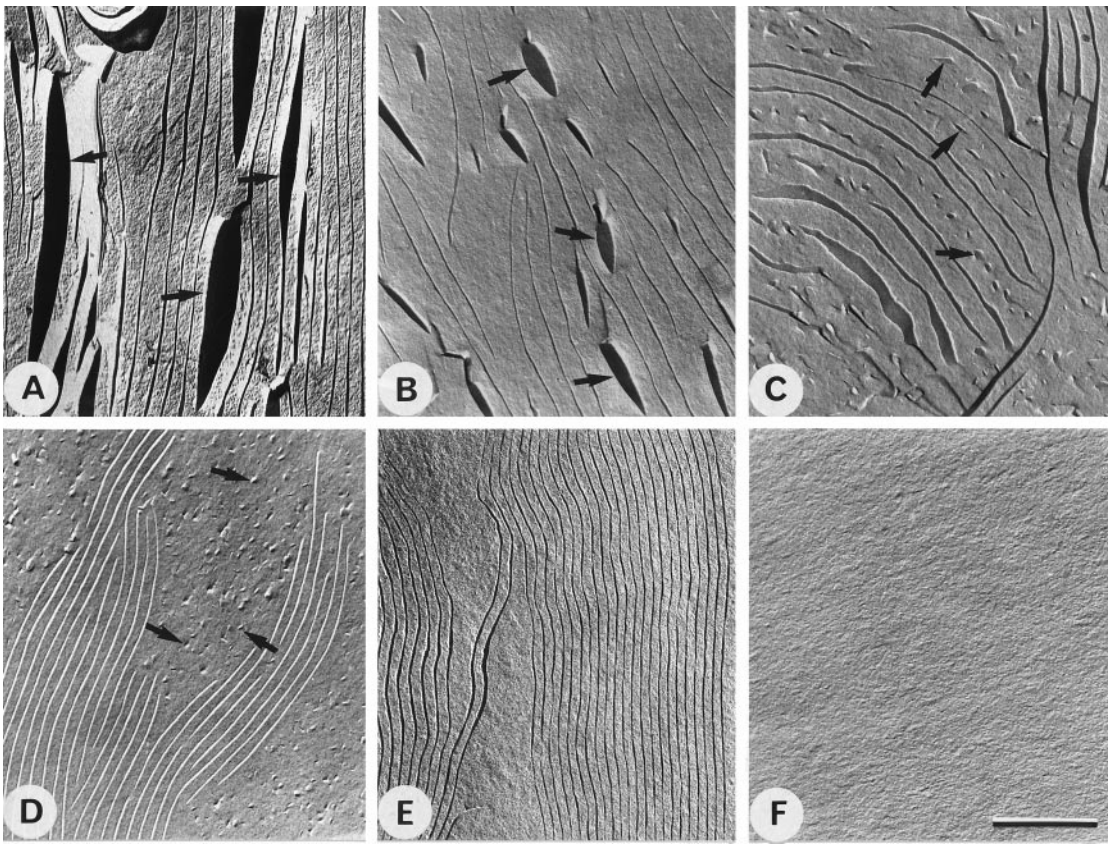

Fig. 3. Coexistence of discs of finite size with a lamellar phase observed by freeze-fracture electron microscopy. (**A**) A swollen (L_β^+) phase (periodicity 64 nm) coexists with large discs of diameter 2 to 3 μm ($r = 0.447$ and $c = 3.9\%$). (**B**) At higher charge ($r = 0.43$), discs shrink to 250 nm and the periodicity of the coexisting lamellar phase is 100 nm. (**C**) At $r = 0.416$, average disc diameter (40 nm) is smaller than the smectic periodicity, producing local segregation. (**D**) Microphase separation between discs of diameter 30 nm and a smectic of periodicity 46 nm occurs for $r = 0.39$. (**E**) At $r = 0.319$, the large excess of cationic surfactant induces formation of micelles coexisting with the lamellar phase. (**F**) Only giant micelles are present for $r < 0.1$. Bar = 500 nm. Shadowing method ensures that objects observed are discs and not pores.

nanodiscs corresponds to a concentration of $c > 60\%$—that is, D^* spacings of 6 nm. When r decreases, the lamellar phase in equilibrium with uncorrelated discs swells up to D^* spacings of 80 nm. At $r < 0.35$, the (L_β^+) phase is in equilibrium with giant wormlike micelles. Osmotic equilibrium between coexisting phases imposes a rapid shrinking of the maximum swelling of the lamellar phase, as previously observed in other surfactant two-phase regions (*18*). At low myristic acid content ($r < 0.1$), only giant micelles are obtained.

The charged (L_β^+) phase (Fig. 1A, II) swells up to spacings of hundreds of angstroms, even with frozen hydrocarbon chains (Fig. 2). The macroscopic appearance is a clear birefringent gel. For most phospholipids in the frozen (L_β) state, including mixtures of charged and uncharged phospholipids, swelling is limited to water thicknesses of only a few nanometers, 10 times smaller than those reported here. This unique swelling property of the catanionic (L_β^+) phase with hydroxide counterions results from the absence of dispersion forces (*19*).

Only two surfactant microstructures with finite and composition-dependent sizes have been described. Finite-sized needles of defined persistence length (*5*) were obtained in a pure catanionic system and discs were obtained in the presence of excess salt (*20*). Mixing long- and short-chain zwitterionic phospholipids produced uncharged discs orienting in a magnetic field (*21*). Rigid colloidal particles are known to appear as fibers, helices, or multilayered tubules made from flat sheets (*22*). To our knowledge, no microstructure of dispersed isolated flat discs with a thickness of nanometers and a controllable diameter from 30 nm well into the micrometer range has been reported.

The sandwich-like structure of nanodiscs with a rigid outer layer of low charge and ion pairs forming the faces is presented schematically in Fig. 5, assuming simplistic ordering of head groups and compatibility between surface ordering of ionic head groups and frozen chains. Different melting temperatures have been observed recently in another catanionic system for these two surface lattices (*23*).

The morphology obtained with our catanionic mixtures may be used to produce mesoporous materials or to orient solubilized molecules. The size, surface potential, and electrokinetic properties of this new type of rigid colloidal particles may thus be considered for molecular templating (*14*). The nematic phase of the rigid nanodiscs contains an unexpectedly high amount of water (up to 95%). This may be used to obtain the anisotropic movement needed to deduce bond angles from nuclear magnetic resonance shifts for nonpolar molecules dissolved in the solvent, such as oligopeptides (*24*). Finally, it is likely that this type of stiff catanionic disc could be used as an easy-to-remove template surface for polymerization of inorganic oxides—for example, as flat or folded silica discs of nanometer thickness (*25*).

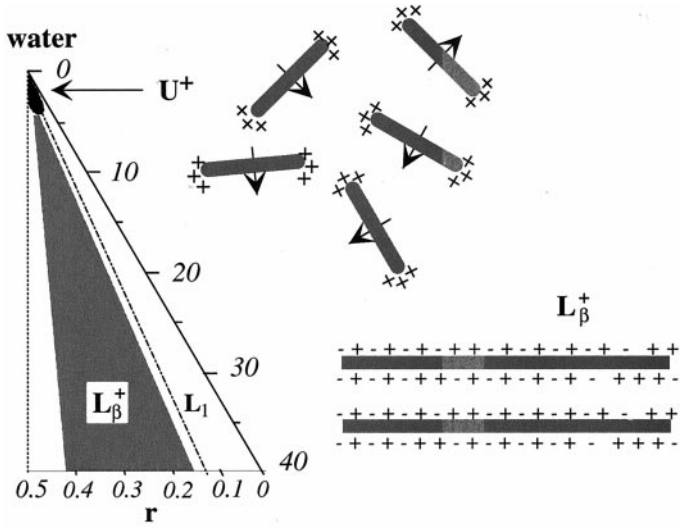

Fig. 4. Equilibrium-phase diagram established in contact with atmospheric CO_2, showing giant micelles (L_1), lamellar phase with frozen chains (L_β^+), and stability region of unbound freely rotating nanodiscs (U^+). The nematic region is observed only in the absence of CO_2 (not shown). The molar ratio $0 < r < 0.5$ and the total surfactant concentration $0\% < c < 40\%$ are given.

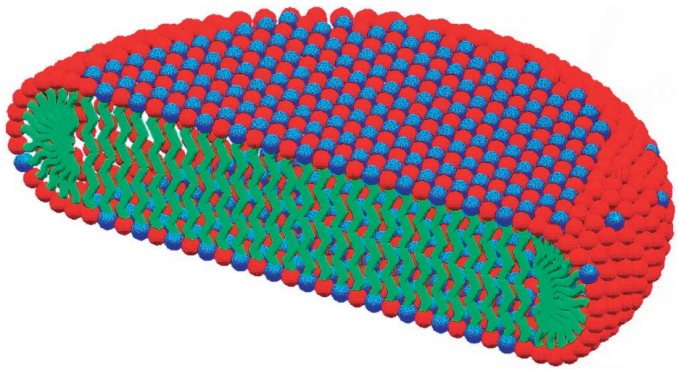

Fig. 5. Schematic view of the sandwich-like microstructure of a nanodisc. Inner layer contains crystallized hydrocarbon chains. Faces are built from ion pairs, which act as double-tailed zwitterionic surfactants forming bilayers. The catanionic component is red.

References and Notes

1. E. W. Kaler, A. K. Murthy, B. E. Rodriguez, J. A. Zasadzinski, *Science* **245,** 1371 (1989).
2. A. Khan and E. Marquès, in *Specialist Surfactants*, I. D. Robb, Ed. (Chapman & Hall, Glasgow, 1997), p. 37.
3. O. Södermann, K. L. Herrington, E. W. Kaler, D. D. Miller, *Langmuir* **13,** 5531 (1997).
4. E. W. Kaler and K. L. Herrington, *J. Phys. Chem.* **96,** 6698 (1992); L. L. Brasher and E. W. Kaler, *Langmuir* **12,** 6270 (1996).
5. H. Hoffmann, J. Kalus, B. Schwander, *Ber. Bunsenges. Phys. Chem.* **91,** 99 (1987).
6. R. G. Laughlin, *The Aqueous Phase Behavior of Surfactants* (Academic Press, New York, 1994).
7. Capillary electrophoresis analysis of the impurity ions present in the commercial form of the surfactant (Fluka) has shown that, in myristic acid, the ionic impurities are sodium (0.1% molar fraction) and calcium (0.05% molar fraction). An aqueous solution (0.1 M) of the bromide form of the surfactant (Sigma) was mixed with Ag_2O powder, the precipitated silver bromide was centrifuged (20,000 rpm), and the only detectable impurity in the remaining solution was bromide at <0.1%. The ion exchange with hydroxide is >99%.
8. M. Dubois and Th. Zemb, *Langmuir* **7,** 1352 (1991).
9. Control scattering experiments have shown that the only effect of adding glycerol is to change the value of r at which aggregates form from micelles or lamellar phases to slightly smaller r values, as expected because of the lower dielectric permittivity of the solvent.
10. J. N. Israelachvili, *Intermolecular and Surface Forces* (Academic Press, London, 1992).
11. A. Tardieu, V. Luzzati, F. C. Reman, *J. Mol. Biol.* **75,** 711 (1973).
12. Because of the absence of salt, the osmotic pressure could be measured with a standard membrane osmometer (Knauer A0278).
13. D. M. Le Neveu, R. P. Rand, V. A. Parsegian, D. L. Gingell, *Biophys. J.* **18,** 209 (1977).
14. S. W. Hyde *et al.*, *The Language of Shape* (Elsevier, Amsterdam, 1997).
15. P. Fromherz, *Ber. Bunseneges. Phys. Chem.* **85,** 891 (1985).
16. S. Safran, P. Pincus, D. Andelmann, *Science* **248,** 354 (1990).
17. N. C. Lockhart, *J. Colloid Interface Sci.* **74,** 509 (1980).
18. F. Ricoul *et al.*, *Eur. Phys. J.* **4(3),** 333 (1998).
19. B. W. Ninham, *Langmuir* **13,** 2097 (1997).
20. K. Tamori *et al.*, *Colloid Polymer Sci.* **270,** 885 (1992).
21. R. R. Vold and R. S. Prosser, *J. Magn. Reson. B* **113,** 267 (1996).
22. J. H. Furhop and W. Helfrich, *Chem. Rev.* **93,** 1565 (1993).
23. K. Horbaschek, H. Hoffmann, C. Thunig, *J. Colloid Interface Sci.* **206,** 439 (1998).
24. N. Tjandra and A. Bax, *Science* **278,** 1111 (1997).
25. M. Dubois and B. Cabane, *Langmuir* **10,** 1615 (1994); K. M. McGrath, D. M. Dabbs, N. Yao, I. A. Aksay, S. M. Gruner, *Science* **277,** 552 (1997).

26. J.-Cl. Dedieu is acknowledged for his help during the electron microscopy experiments. The authors are grateful to B. Ninham and to the referees for their useful suggestions.

13 July 1998; accepted 14 December 1998